Journal of Catalysis **204,** 378–392 (2001)
doi:10.1006/jcat.2001.3374, available online at http://www.idealibrary.com on IDEAL®

Reaction Kinetics on Heterogeneous Model Catalysts

The CO Oxidation on Alumina-Supported Pd Particles

J. Hoffmann, I. Meusel, J. Hartmann, J. Libuda,[1] and H.-J. Freund

Fritz-Haber-Institut der Max-Planck-Gesellschaft, Faradayweg 4-6, D-14195 Berlin, Germany

Received April 19, 2001; revised August 3, 2001; accepted August 4, 2001

We have employed multimolecular beam techniques to study the transient and steady-state kinetics of the CO oxidation on alumina-supported Pd model catalysts as a function of particle size and surface structure. The model systems were prepared under UHV conditions on a well-ordered alumina film on NiAl(110) and were previously characterized with respect to their geometric and electronic structure and their morphology. Crossing two molecular beams on the sample surface we have systematically probed the CO_2 production rate over a wide range of reactant fluxes and at different sample temperatures. Characteristic differences as a function of particles size are observed in both the transient and steady-state regime. In order to relate these effects to the differences in structure and adsorption properties, we have performed microkinetic simulations of the entire series of transient experiments. Whereas it is found that the kinetics on large and ordered Pd particles can in general be described by a homogeneous surface model, significant deviations remain with respect to the kinetics on small and defect-rich particles. In order to semiquantitatively simulate these effects, we consider a heterogeneous surface model, which takes into account the simultaneous presence of different types of adsorption sites. Depending on their distribution, surface diffusion between these sites is included. It turns out that the differences observed for the small particles can be qualitatively understood by a simple model, where we add a small fraction of weakly CO binding sites to the regular adsorption properties. This type of modified adsorption behavior is in agreement with previous desorption studies.

1. INTRODUCTION

Can we understand the reaction kinetics on complex surfaces such as supported catalysts on a molecular basis? Considering the fact that even for simple, single crystal surfaces detailed reaction mechanisms and their kinetics could be successfully disentangled only for very few reaction systems, the task appears even more demanding on complex nanostructured surfaces. In particular in the case of supported metal particle catalysts, it has early been recognized that a large number of unique effects might come into play, the role of which would have to be understood in detail in order to describe the kinetics on such systems and their deviation from simple surfaces (1). Among these effects which have been discussed are, for example, size effects related to the electronic structure of small paticles, geometric effects related to the presence of specific adsorption sites, and contributions connected to adsorption, reaction, spillover, or interaction with the support.

In practice, it is most important to realize that a certain degree of complexity is an inherent property of most catalytic surfaces, and the kinetic effects related to this complexity cannot be fully understood on the basis of single crystal experiments only. Recently, illustrative examples have been given by Zhdanov and Kasemo (2–4), who performed Monte Carlo calculations on the reaction kinetics of heterogeneous surfaces coupled by surface diffusion and demonstrated that such coupling effects may be essential for an understanding of the kinetics.

In spite of these theoretical attempts and concepts, experimental examples which have clearly demonstrated such effects on complex surfaces are extremely scarce. This lack of data is related to serious experimental difficulties, which are in fact twofold: First, there is the vast *complexity* of supported catalysts containing a large number of nonequivalent adsorption sites, which are typically difficult to characterize (e.g., different facets, edges, corner sites, defects, metal-support interface sites, and possibly different types of support sites). Second, there is a serious experimental difficulty related to the problem that *systematic and quantitative kinetic data* have to be obtained under extremely well-controlled conditions.

In order to overcome the first problem a variety of supported model catalysts have been developed. These systems are based on metal single crystals or ordered oxide films and are characterized by a reduced and controllable degree of complexity (see, e.g., (5–9) and references therein). Moreover, most surface science techniques can be applied to these models and can provide most detailed structural

[1] To whom correspondence should be addressed. E-mail: libuda@fhi-berlin.mpg.de. Fax: +49-30-8413-4309.

0021-9517/01 $35.00

information. In this study, the experiments were performed on Pd particles supported on an ordered Al_2O_3 model film, which is prepared on a NiAl(110) single crystal. The structure and defects of the oxide film (10, 11) as well as the growth, geometric, and electronic structure of Pd particles supported on this film and their adsorption properties have been studied previously (6, 9, 12) and the results will be used in connection with the interpretation of the reactivity studies presented here.

Once we have developed suitable model systems, we arrive at the second problem, which is related to the question of how we can perform quantitative kinetic measurements on these systems under suitably well-controlled conditions. With regard to this issue, it has early been recognized that with respect to kinetic studies on a molecular level molecular beam techniques represent the method of choice (see, e.g., (13–15)). The unique features of kinetic beam experiments are essentially connected to its single scattering characteristics, which allow, e.g., precise high frequency modulation, quantitative analysis of surface processes, and control and analysis of the dynamic properties of incoming and desorbing molecules.

Due to the combination of experimental difficulties, the number of molecular beam studies on supported model systems is scarce. The previous work involved the adsorption and oxidation of CO on Pd (16–27) and Rh (28–30) particles as well as the adsorption and reactivity of NO (31, 32). Most work, however, has been restricted to relatively simple beam experiments and a very limited range of parameters, so far. Thus, we have started to perform systematic molecular beam experiments on the CO oxidation on $Pd/Al_2O_3/NiAl(110)$ in combination with in situ infrared reflection absorption spectroscopy (IRAS) (33–37). As previously suggested by Becker and Henry (18, 19), it is found that in particular the transient reaction behavior may be used as a sensitive tool to indicate differences in the kinetics with respect to simple homogeneous surfaces. Specifically, we have shown in a recent study that the transient reaction behavior is drastically dependent on particle size and morphology (36). However, these combined molecular beam/time resolved IRAS experiments demonstrated that kinetic effects on these complex model surfaces cannot always be intuitively understood in a straightforward manner. A detailed analysis might be required which to a certain degree takes into account the complexity of the system. This is particularly the case, if the model catalyst is characterized by an increasing degree of heterogeneity, e.g., particles of different size, morphology, and surroundings, or particles containing a variety of nonregular adsorption sites such as steps, corners, or defects.

In order to qualitatively understand the differences in the steady-state and transient reactivity, we reconsider the molecular beam data on the CO oxidation $Pd/Al_2O_3/NiAl(110)$ and extend the previous kinetic modeling of the experiment. We take into account not only regular adsorption sites but also defect adsorption with modified activation barriers for desorption and reaction. Depending on whether the different adsorption sites are located on a common particle or on isolated particles, we take into account equilibration of the local CO coverages via diffusion. It turns out that all the modifications in both the steady-state and transient behavior calculated on the basis of the extended model are qualitatively consistent with the experimental observations.

2. EXPERIMENTAL RESULTS

Before discussing the kinetics of the model reaction, we will briefly consider the structure of the model catalysts, as far as it is necessary for the following discussion. Subsequently, we will summarize the results of kinetic experiments employing multimolecular beam techniques and in situ IR reflection absorption spectroscopy.

2.1. Pd Model Catalysts

Briefly, the supported model catalysts were prepared by sputtering and annealing of a NiAl(110) single crystal, followed by an oxidation and annealing procedure, the details of which are given elsewhere (10, 11). Before the actual experiment, the active metal component was deposited by evaporation in UHV under exactly controlled conditions. Details concerning typical deposition rates and conditions are given in Table 1. After preparation the Pd particles were stabilized by oxygen and CO exposure as discussed previously (33). The growth and structure of the $Pd/Al_2O_3/NiAl(110)$ system in general (6, 9, 38, 39) and the specific Pd model catalysts employed in this work (33, 36) have been discussed extensively and we refer to the literature for further details.

In the following we will specifically consider the reactivity of two types of particles:

- Type I particles: These particles were grown at a sample temperature of 300 K. Under these conditions well-ordered Pd crystallites are formed, which grow in (111) orientation and preferentially expose (111) facets. For the Pd coverage used here, the particle density amounts to 1×10^{12} particles cm^{-2} and the particles diameter can be estimated as 5.5 ± 0.7 nm. The particles will contain an average of 2700 Pd atoms.
- Type II particles: The second type of Pd particles were grown at a substrate temperature of 90 K. Under these conditions, the reduced mobility of the Pd atoms results in an increased nucleation density, resulting in the formation of smaller islands. For the model system under consideration the mean island diameter was 1.8 ± 0.4 nm and the particle density was 6.5×10^{12} particles cm^{-2}. These particles contain an average of 100 Pd atoms. Most importantly, however, neither scanning tunneling microscopy (STM) nor high resolution low electron energy diffraction (LEED) reveal

TABLE 1

Preparation Conditions and Structural Parameters for the Pd Particles on Al_2O_3/NiAl(110)

	Type I Pd Particles	Type II Pd Particles
	Deposition parameters	
Pd coverage (atoms · cm^{-2})	2.7×10^{15}	0.7×10^{15}
Deposition temperature (K)	300	90
Deposition rate (atoms · $cm^{-2} \cdot s^{-1}$)	9×10^{12}	$5 - 9 \times 10^{12}$
	Structural parameters	
Island density (cm^{-2})	$1.0\ (\pm 0.2) \times 10^{12}$ (6, 33)	$6.5\ (\pm 2) \times 10^{12}$ (12)
Number of Pd atoms/island	~2700 (6, 33)	~100 (12)
Estimated fraction of support covered by Pd	~0.20 (±0.02)	~0.15 (±0.05) (36)
Estimated fraction of surface Pd atoms	0.20 (±0.03)	0.6 (±0.1) (36)
Average island size	~5.5 ± 0.7 nm (6, 36)	~1.8 ± 0.4 nm (36)
Epitaxial orientation	(111) (6)	—
Island structure	Crystalline, predominantly (111) facets, small fraction of (100) facets (6, 39)	Irregular, no indications for ordered facets, hemispherical (6)

any indication for the formation of ordered facets on these small aggregates, indicating a more irregular and defect rich surface. We may anticipate that the modified adsorption properties of these particles (see below) are to a large extent related to these differences in the surface structure.

For clarity, the structural data on the two types of model catalysts have been summarized in Table 1. Typical STM images together with a summary of the reactivity data are displayed in Fig. 1. Before the kinetic experiments were performed the particles were stabilized by oxygen exposure under reaction conditions (33, 35, 40). This procedure, which is necessary to obtain stable reaction kinetics, is connected to a bulk diffusion process under reaction conditions, but has been shown to affect neither the particle density nor the morphology to a significant extent (33).

With respect to the kinetic simulation in Section 3, it is important to note that distinct differences with respect to the CO adsorption properties have been observed for the two types of model systems. Both thermal desorption spectroscopy (40) and molecular beam relaxation spectroscopy (35, 40) indicate that on the smaller particles, we find a slightly stronger bonding of CO at low CO coverage. The main difference with respect to the CO adsorption properties is, however, observed at large coverages, where it is found that with decreasing particle size an increasing fraction of weakly bonding adsorption sites can be populated (6, 9). These observations are consistent with recent calculations, which show only slight increases in the adsorption energy for CO on Pd step or edge sites (41). Once those sites are occupied, CO has to bond to less favorable sites. In particular terminal adsorption geometries are strongly disfavored for the CO–Pd system, which may enhance the coverage dependence that principally arises from repulsive CO–CO interactions (see, e.g., (5) and references therein).

We may summarize these observations by concluding that with decreasing particle size, we find an increasing coverage dependence of the CO adsorption strength. In other words: On small particles and at *low coverage* adsorption sites are occupied, which show a *slightly enhanced adsorption strength,* whereas *at higher coverage* a large fraction of *more weakly adsorbing* sites are populated. This information will be used in the extended kinetic model in Section 3.2.

2.2. Molecular Beam Experiments: Transient and Steady-State Kinetics

In this section we will briefly review the molecular beam experiments, which are the subject of the kinetic simulation in Section 3. All experiments were performed in a UHV molecular beam/surface spectroscopy apparatus at the Fritz-Haber-Institute (Berlin), which has been described in the literature recently (42). The system has been specifically designed for kinetic studies on complex model systems and offers the experimental possibility of up to three beams being crossed on the sample surface. The CO and O_2 beams, which were used in the work presented here, are generated by two effusive sources based on multichannel arrays. The beam sources allow an easy variation of the beam intensities over several orders of magnitude without any change in the beam properties. Beam modulation is provided by a computer-controlled shutter located inside the second pumping stage of the beam sources. Angular-integrated, gas phase measurements were performed with a quadrupole mass spectrometer which is not in the line of sight of the sample.

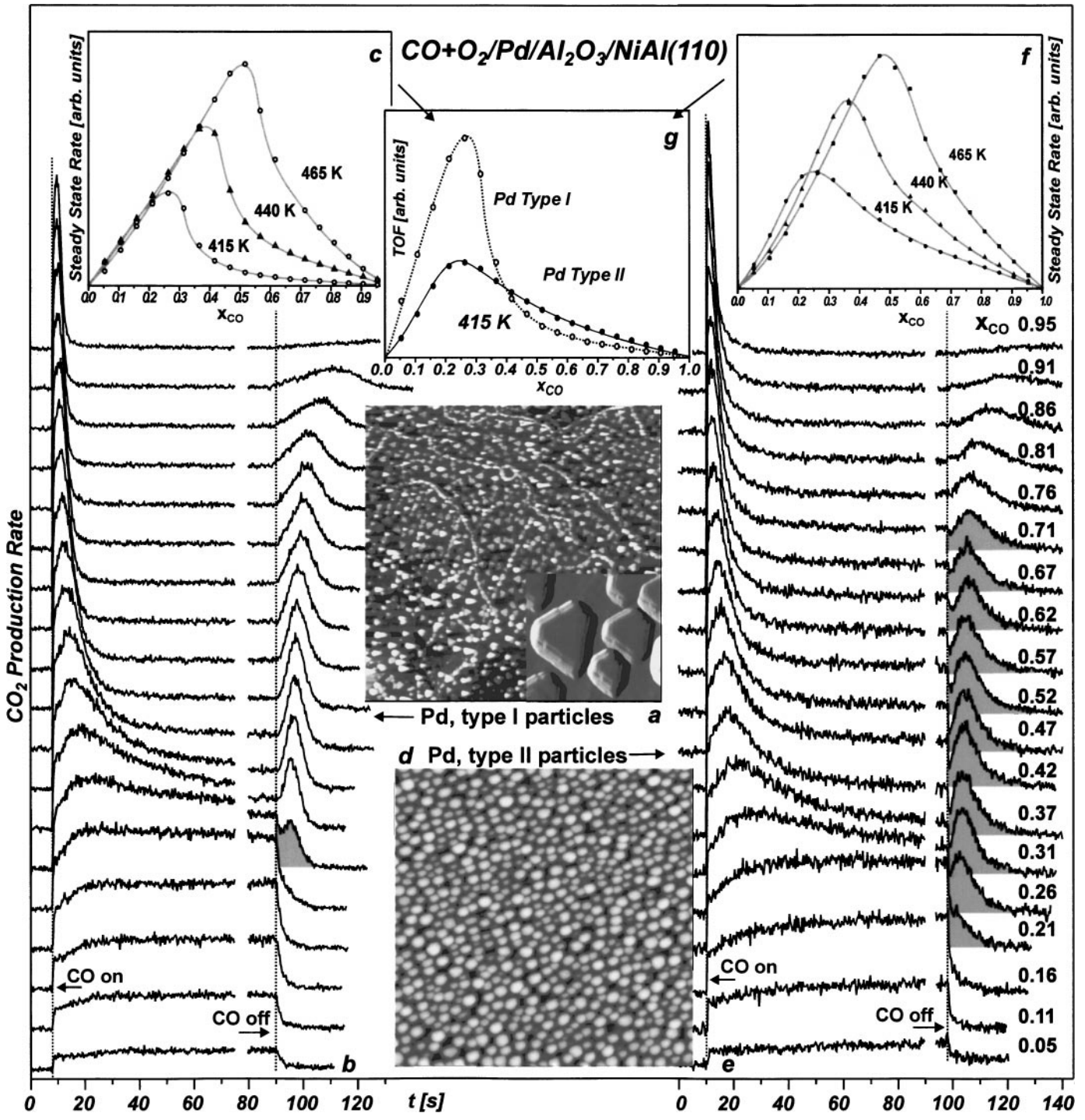

FIG. 1. (a) STM image (3000 × 3000 Å) of Pd particles of type I (see text) on Al_2O_3/NiAl(110); the inset shows a differentiated closeup (200 × 200 Å) (33); (b) transient behavior of the CO_2 production rate (continuous O_2 beam and a modulated CO beam) as a function of the CO fraction in the total gas flux x_{CO} (T_{Sample} = 415 K, $p_{total} = 1.0 \times 10^{-6}$ mbar) for the type I Pd deposits (36); (c) steady-state reaction rates as a function of the CO flux fraction x_{CO} for the type I particles ($p_{total} = 1.0 \times 10^{-6}$ mbar) (35); (d) STM image (1000 × 1000 Å) of Pd particles of type II on Al_2O_3/NiAl(110) after heating to 500 K (36); (e) as (b) for the type II particles (36); (f) as (c) for the type II particles (36); (g) comparison of the turnover frequencies (TOF) for the CO oxidation on the type I and type II Pd particles on Al_2O_3/NiAl(110) (36).

We will mainly focus on the reaction rate differences, which can be observed under steady-state and transient conditions. A more detailed discussion of the experimental results, including also in situ IRAS data, can be found elsewhere (35–37). A summary of the kinetic experiments for both types of Pd catalysts is given in Fig. 1. In general, we use two effusive beams—O_2 and CO—of variable intensity crossed on the sample surface. The O_2 beam impinges on the surface in a continuous fashion. At a given time (marked in the traces in Fig. 1), we switch on the CO beam and the CO_2 production rate is monitored. The intensity of the two beams is chosen such that the total effective pressure

$$p_{total} = p_{CO} + p_{O_2} \quad \text{with} \quad p_i = F_i(2\pi m_i kT)^{0.5} \qquad [1]$$

at the sample position is constant for all experiments (1×10^{-6} mbar for the experiments shown in Fig. 2). However, we vary the fraction of CO

$$x_{CO} = \frac{F_{CO}}{F_{CO} + F_{O_2}} \qquad [2]$$

in the total flux $F_{CO} + F_{O_2}$. It is observed that after switching on the CO beam a steady-state reaction rate is established after an initial transient period of variable length. These steady-state reaction rates as a function of the CO flux fraction are plotted in the insets in Figs. 1c and 1f for different reaction temperatures and both types of particles. Finally, after the steady state has been reached, the CO beam is switched off, resulting in a second transient region in the CO_2 production traces.

Depending on the CO flux fraction x_{CO}, two different types of transient behavior can be distinguished. The corresponding flux regimes will be denoted as the O-rich regime and the CO-rich regime.

- The oxygen-rich reaction regime (low x_{CO} values): In the oxygen-rich reaction regime, we start from an oxygen saturated surface. Upon switching on the CO beam, we immediately find substantial CO_2 production (on the time scale of the experiment). Subsequently, the reaction rate increases slowly toward the steady-state rate. The duration of this characteristic transient period depends on the total and partial reactant fluxes and the reaction temperature (for the experiments shown in Fig. 1 typically on the order of 20 s). The initial rise of the reaction rate is related to the probability of the trapped CO precursor to chemisorb on the oxygen saturated particle. This chemisorption probability increases, once oxygen vacancies are produced by the proceeding reaction, which leads to the slow increase of reaction rate toward the steady state. A more detailed discussion of the related processes can be found in the literature (16). Note that the steady state under these conditions is characterized by a high O and a low CO coverage. Once the CO beam is switched off, the CO on the surface is consumed and the reaction rate drops rapidly.
- The CO-rich reaction regime (high x_{CO} values): If the analogous experiment is performed under CO-rich

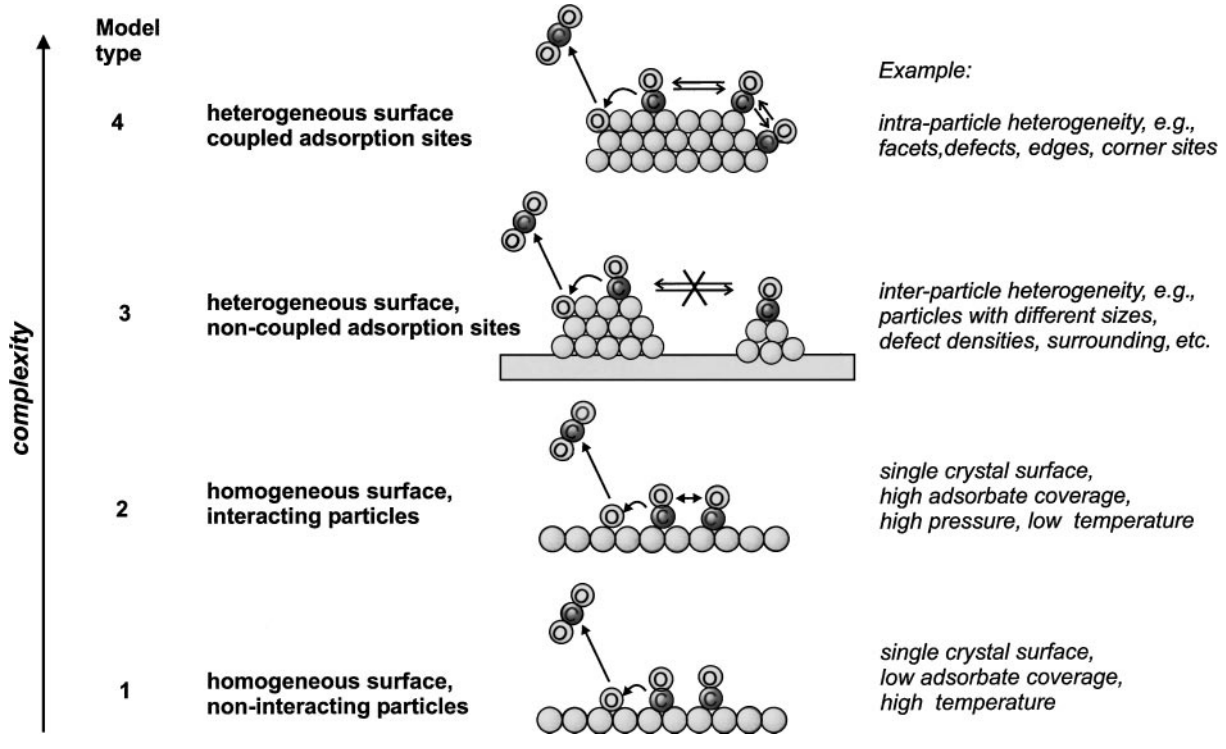

FIG. 2. Schematic representation of the considered kinetic models.

conditions, we again start from an oxygen saturated surface. The initial behavior upon switching on the CO beam is similar to the behavior discussed before for high oxygen flux. It is characterized by an instantaneous onset of the reaction, followed by a slower change toward the steady-state conditions. In contrast to the oxygen-rich case, however, we observe that the CO_2 production rate passes through a maximum. This behavior is caused by an increasing CO coverage, finally inhibiting the dissociative adsorption of O_2; i.e., the surface is poisoned by CO (see, e.g., (43) and references therein). Consequently, the steady state will be characterized by a high CO and a low O coverage. Once the CO beam is switched off, the CO, which has been accumulated on the surface, will be consumed. The surface reaction will again produce vacant adsorption sites, which itself increases the O_2 adsorption rate and thus also the total reaction rate. Consequently, a second transient CO_2 production peak evolves after switching off the CO beam.

The two reaction regimes (O-rich and CO-rich) can be easily identified in the steady-state plots in Fig. 1 as well: Starting from O-rich conditions the steady-state reaction rate increases with increasing CO flux fraction, until a critical CO/O_2 ratio is reached at which the system switches to a CO-rich steady-state. This point at which the CO poisoning becomes dominant is connected with a steep drop in reaction rate.

If we now closely inspect the CO_2 reaction rates for the large particles (type I) under reaction conditions in between the two reaction regimes, we observe a third type of behavior. The corresponding transient region is highlighted in Fig. 1 (area shaded in gray). Here, we observe that upon switching off the CO beam, the reaction rate first drops rapidly, but is followed by evolution of a smaller CO_2 peak. Previously, it was suggested that this behavior may be directly related to the presence of strongly binding adsorption sites for CO (18, 19). It was anticipated that upon termination of the beam, CO may rapidly desorb from the regular facets, followed by a reaction of CO adsorbed on the defects on which adsorption might be stronger. In a series of combined molecular beam/time-resolved IRAS experiments, however, we have recently shown that the sudden drop in the reaction rate is not correlated to a sudden drop in the CO-induced IR absorption features (35). In light of these results, the hypothesis that the transient feature is correlated to rapid CO desorption from facets appears unlikely. In an attempt to explore alternative explanations, we have simulated the transient experiment assuming a homogeneous surface (see also Section 3.1 (35)). It can be shown that a similar dip in the reaction rate may trivially appear as a consequence of the competition of oxygen adsorption and CO consumption in the transient region. However, this dip is typically significantly less pronounced than the effect observed experimentally. At this point it appears likely that in order to fully account for the transient and steady state behavior a homogeneous surface model is insufficient and different types of heterogeneity have to be taken into consideration explicitly.

In order to probe the role of defects experimentally, we perform an identical set of transient experiments on both types of Pd model system (type II particles, Fig. 1e, vs type I particles, Fig. 1b). If we compare the CO_2 traces for the two systems, we observe a qualitatively similar behavior in the limiting cases of very high and very low CO flux fractions. In the intermediate range, however, pronounced differences appear:

- The most obvious effect is related to the transient behavior upon switching off the CO beam. Here, the so-called transition behavior, with a dip in the reaction rate being followed by a peak in the CO_2 production, appears over a very broad range of flux conditions ($0.21 \leq x_{CO} \leq 0.71$, highlighted areas in Fig. 1e). Please note that we have performed similar, time-resolved IRAS experiments in the transient region for the small particles of type II as were previously published for the large particles of type I (35). It turns out that also for the small particles the sudden drop in the rate is not correlated to a sudden change in the CO absorption spectrum. This indicates that also for the small Pd particles (type II) the effect is not related to a sudden loss of a large fraction of the adsorbed CO.
- The second difference is related to the intensity of the transient peak after the CO beam is switched off in comparison to the level of the steady-state rate. Here, the transient peak is much weaker for the small particles of type II in comparison to the larger Pd crystallites of type I.
- The third dissimilarity between the two types of metal aggregates can be observed by comparing the steady-state rates as a function of the CO fraction x_{CO} (Figs. 1c and 1f). The differences become more apparent if we directly compare the turnover frequencies (TOF) by relating the reaction rates to the number of surface sites (as derived from STM and high resolution LEED data (6, 44)). This comparison, which is shown in Fig. 1g, reveals that under O-rich conditions the TOF of the small particles (type II) is lower as compared to the larger particles of type I. Under CO-rich conditions, however, the relationship reverses; i.e., the poisoning effect of CO appears to be significantly less pronounced on the small aggregates. The origin of the reduced activity under oxygen-rich conditions is unclear and has recently been discussed elsewhere (33, 36). A possible explanation may be related to differences in the oxygen interaction with the small defect-rich aggregates. However, the absolute differences in the TOF values are moderate and as the limited accuracy of the structural data results in some uncertainty in the absolute values, we will mainly focus on the *shape* of the TOF curve rather the *absolute differences*. Here, the reduced CO poisoning under CO-rich conditions is the central issue and we may now explore how

this effect is related to the differences in the CO adsorption properties discussed in Section 2.1.

In order to obtain a qualitative understanding of these effects, we have modeled the transient experiments, extending the previous homogeneous surface model to heterogeneous surfaces.

3. MICROKINETIC SIMULATIONS

In the previous section we have shown that characteristic differences as a function of particle size are observed with respect to both the transient and steady-state behavior in the beam experiment. How can the origin of these difference be explored in terms of microkinetic simulations?

The direction in which we develop the modeling is schematically illustrated in Fig. 2. As a starting point we may consider a simple mean field model of a homogeneous surface (Fig. 2, model type 1). In this simplest of all cases we assume that the adsorbate molecules are randomly distributed on the surface and we neglect all lateral interactions. Previously, we have shown that the steady-state and transient kinetics on the large and ordered particles (type I) can be semiquantitatively understood on the basis of such an assumption, if we use the available kinetic parameters from single crystal measurements as an input (35).

Due to the simplicity of the model, however, certain discrepancies remain. In an attempt to improve the model, the first additional factors which have to be taken into account are the relatively strong lateral interactions between the adsorbate molecules (Fig. 2, model type 2). Such interaction may, e.g., result in (a) strong coverage dependencies of the activation barriers for desorption (45) and reaction (43, 46) and (b) a nonhomogeneous adsorbate distribution (e.g., islanding), in particular at low reaction temperatures (see, e.g., (47)). Whereas a microscopic description of the latter effect in two dimensions requires Monte Carlo type simulations (see, e.g., (2)), the coverage dependence of the activation barriers may to a first approximation be taken into account within a simple mean field approach (see, e.g., (48) and references therein). Naturally, considering these coverage dependencies results in a significantly improved description of the temperature dependence of the steady-state rates. However, qualitative deviations remain with respect to the transient experiments and the small particles of type II.

At this point it becomes obvious that any improved description will require the heterogeneity of the model system to be considered. Here, we may differentiate between two different classes of heterogeneity, which we will denote as *interparticle* and *intraparticle* heterogeneity. In the first case we are dealing with individual metal particles which as such may be characterized by differing adsorption and reaction rates (e.g., due to varying defect densities, particles sizes, and surroundings). As the particles are largely decoupled by weakly adsorbing support areas in between, we may regard them as individual reactors without significant exchange of adsorbates by surface diffusion (Fig. 2, model type 3).

Additionally, we may take into account that different types of adsorption and reaction sites are present on each individual particle (intraparticle heterogeneity, Fig. 2, model type 4). These different sites may, for example, be different facets of a crystallite, edge, and corner sites, interface sites at the particle borderline, or structural or chemical defects of any other type. An important difference with respect to the first type of heterogeneity is that adsorbates within a single particle may be rapidly exchanged by surface diffusion. In the case of the CO oxidation reaction and under the condition considered in this work, we may assume that exchange of CO by surface diffusion between different sites on a single particle is fast with respect to the LH reaction, whereas diffusion of adsorbed oxygen is a considerably slower process (again with respect to the LH step; for an estimate of diffusion energies see, e.g., (49)).

In Section 3.2, we will consider the influence of both types of heterogeneity on the transient and steady-state reaction rates, applying a simple multiadsorption state, mean field model for a heterogeneous surface to the beam experiments. As a starting point we will briefly review the results derived by a mean-field model based on a perfectly homogeneous surface (35).

3.1. Homogeneous Surface Models

To start with we may expand the overall CO oxidation reaction in its elementary steps (see also the schematic representation in Fig. 3):

$$\mathrm{CO(g)} \leftrightarrow \mathrm{CO(a)} \quad [3]$$

$$\mathrm{O_2(g)} \rightarrow \mathrm{2O(a)} \quad [4]$$

$$\mathrm{CO(a) + O(a) \rightarrow CO_2(a) \xrightarrow{fast} CO_2(g).} \quad [5]$$

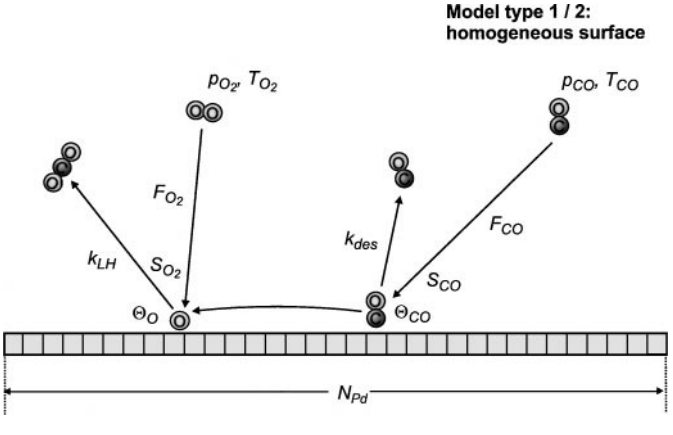

FIG. 3. Kinetic parameters in the homogeneous surface models.

TABLE 2

Parameters Used in the Kinetic Simulations

Parameter	Model type 1	Model type 2	Model type 3	Model type 4	Ref.
S^0_{CO}	0.96	0.96	0.96	0.96	For Pd(111), see (50)
$S^0_{O_2}$	0.78	0.78	0.78	0.78	For Pd(111), see (50)
	-7.4×10^{-4} T_s	-7.4×10^{-4} T_s	-7.4×10^{-4} T_s	-7.4×10^{-4} T_s	
$\theta^{max}_{CO(,1)(,2)}$	0.5	0.5	0.5	0.5	For Pd(111), see (51)
$\theta^{max}_{O(,1)(,2)}$	0.25	0.25	0.25	0.25	For Pd(111), see (51)
C_{T_S}	0.3	0.3	0.3	0.3	See text
N_{Pd} ($cm^{-2}\,s^{-1}$)	1.53×10^{15}	1.53×10^{5}	0.54×10^{15}	0.54×10^{15}	
α_1	(1)	(1)	0.9	0.9	
$E_{des(,1)}$ (kJ mol^{-1})	136	136	136	136	134 ± 8 for Pd(111) (50); 136 ± 9 for Pd(type I)/Al_2O_3/NiAl(110) (33)
$\nu_{des(,1)}$ (s^{-1})	$10^{15.0}$	$10^{14.0}$	$10^{14.5}$	$10^{14.5}$	$10^{14.4\pm0.8}$ for Pd(111) (50); $10^{14.9\pm0.9}$ for Pd (type I)/Al_2O_3/NiAl(110) (33)
α_{CO}	0	0.1	0.1	0.1	See text
$E_{LH(,1)}$ (kJ mol^{-1})	60	60	60	60	59 for Pd(111) (46); 62 ± 8 for Pd(type I)/Al_2O_3/NiAl(110) (33)
$\nu_{LH(,1)}$ (s^{-1})	$10^{7.9}$	$10^{7.9}$	$10^{7.7}$	$10^{7.7}$	$10^{7.0\pm1.0}$ for Pd (type I)/Al_2O_3/NiAl(110) (33)
α_2	—	—	0.1	0.1	
$E_{des,2}$ (kJ mol^{-1})	—	—	110	110	See text
$\nu_{des,2}$ (s^{-1})	—	—	$10^{14.5}$	$10^{14.5}$	See text
$E_{LH,2}$ (kJ mol^{-1})	—	—	45	45	See text
$\nu_{LH,2}$ (s^{-1})	—	—	$10^{7.7}$	$10^{7.7}$	See text

As the CO_2 desorption is much faster than its formation, we do not have to take into account adsorbed CO_2, explicitly. Thus, we may convert the reaction system to the following system of coupled differential equations:

$$\frac{d\theta_{CO}}{dt} = \frac{F_{CO}}{N_{Pd}} S_{CO} - k_{des}\theta_{CO} - k_{LH}\theta_{CO}\theta_O \qquad [6]$$

$$\frac{d\theta_O}{dt} = 2\frac{F_{O_2}}{N_{Pd}} S_{O_2} - k_{LH}\theta_{CO}\theta_O \qquad [7]$$

$$r_{CO_2} = \frac{F_{CO_2}}{N_{Pd}} = k_{LH}\theta_{CO}\theta_O. \qquad [8]$$

Here, we have defined the coverages of CO, θ_{CO}, and oxygen, θ_O, as

$$\theta_{CO,O} = \frac{N_{CO,O}}{N_{Pd}} \qquad [9]$$

with N_{Pd} being the density of Pd surface (e.g., $N_{Pd} = 1.53\times10^{15}\ cm^{-2}\ s^{-1}$ for a Pd(111) surface) and $N_{CO,O}$ being the density of adsorbed CO and O, respectively. $F_{CO,O}$ is the flux density of CO and O at the sample position, F_{CO_2} is the flux density of desorbing CO_2, and r_{CO_2} is the CO_2 production rate per Pd surface atom (turnover frequency). For both the LH rate constants k_{LH} and desorption rate constant k_{des} we use a simple Arrhenius type temperature dependence (model type 1):

$$k_{des} = \nu_{des}\exp\left(-\frac{E_{des}}{k_B T_s}\right) \qquad [10]$$

$$k_{LH} = \nu_{LH}\exp\left(-\frac{E_{LH}}{k_B T_s}\right). \qquad [11]$$

In Table 2 we have compiled literature data on the activation energies for desorption E_{des} and reaction E_{LH} and the preexponential factors ν_{des} and ν_{LH} together with all other parameters used in the following simulations.

Next, we model the sticking coefficients of CO S_{CO} and oxygen S_{O_2} using simple (not always realistic) Langmuir laws:

$$S_{CO} = S^0_{CO}\left(1 - \frac{\theta_{CO}}{\theta^{max}_{CO}} - C_{T_S}\frac{\theta_O}{\theta^{max}_O}\right) \qquad [12]$$

$$S_{O_2} = \begin{cases} S^0_{O_2}\left(1 - \dfrac{\theta_{CO}}{\theta^{max}_{CO}} - \dfrac{\theta_O}{\theta^{max}_O}\right)^2; & 1 - \dfrac{\theta_{CO}}{\theta^{max}_{CO}} - \dfrac{\theta_O}{\theta^{max}_O} \geq 0 \\ 0; & 1 - \dfrac{\theta_{CO}}{\theta^{max}_{CO}} - \dfrac{\theta_O}{\theta^{max}_O} < 0. \end{cases} \qquad [13]$$

For the zero coverage sticking coefficients S^0_{CO} and $S^0_{O_2}$ we

will use $S^0_{CO} = 0.96(\forall T_s)$ and $S^0_{O_2} = 0.78 - 7.4 \times 10^{-4}\ T_s$, where T_s is the sample temperature (50). For the maximum coverages, we assume $\theta^{\max}_{CO} = 0.5$ and $\theta^{\max}_{O} = 0.25$. Those values correspond to the saturation coverages on Pd(111) at $T_s \geq 300$ K (51). Deviating from the Langmuir expression, a correction is introduced concerning the influence of preadsorbed oxygen on the sticking of CO($C_{T_s}(\theta_O/\theta^{\max}_O)$, see Eq. [12]), which is physically related to the presence of a precursor to CO chemisorption. Although there is no strong inhibiting effect of preadsorbed oxygen on the sticking of CO on Pd(111)(46), this minor effect has to be taken into consideration to account for the reaction rate at high oxygen coverage and to produce a qualitatively correct transient behavior upon impingement of the CO beam on the oxygen saturated sample (for details see (35), also (16, 48)).

Some typical results of such calculations are plotted in Figs. 4a and 4b. First, we consider the transients in Fig. 4a. A comparison with the experimental data (see also (35)) reveals that the experimental reaction rates are well reproduced in both the CO-rich and the oxygen-rich regimes (see traces for $x_{CO} = 0.1$ and 0.65, respectively). With respect to the discussion of the transient behavior in the transition regime, a minor dip in the reaction rate is observed after the CO beam is switched off. The width of the flux region under which this dip occurs is similar to what is observed experimentally for the Pd particles of type I. However, it is by far not as pronounced as observed in the experiment. We can understand the peculiar transient behavior to be a consequence of the competition between two processes. On the one hand, the reaction rate immediately decreases due to the decreasing CO coverage upon termination of the beam. On the other hand, the oxygen adsorption rate increases due to the decreasing CO coverage. Due to the different kinetics of both processes, the product of the coverages might reach a maximum, giving rise to the CO_2 peak at a later time (35).

The possible origin of the moderate deviations between the simulation and experimental results for the large and ordered type I particles have been discussed, previously (35). As mentioned above, we were recently able to show via time-resolved IRAS that the behavior under discussion is not directly related to the presence of strongly CO binding adsorption sites. Thus, we had to conclude that the transient behavior in this regime cannot be fully understood within the homogeneous surface mean field model. This is corroborated by the observation that the transient behavior sensitively depends on the structural properties of the catalyst, as demonstrated by the comparison with the data on the type II Pd particles. At this point it is noteworthy that near the transition region between the CO-rich and O-rich regime the transient experiments provide a particularly sensitive tool in identifying the kinetics differences of the type discussed here. We will come back to this in connection with the discussion of the heterogeneous surface models.

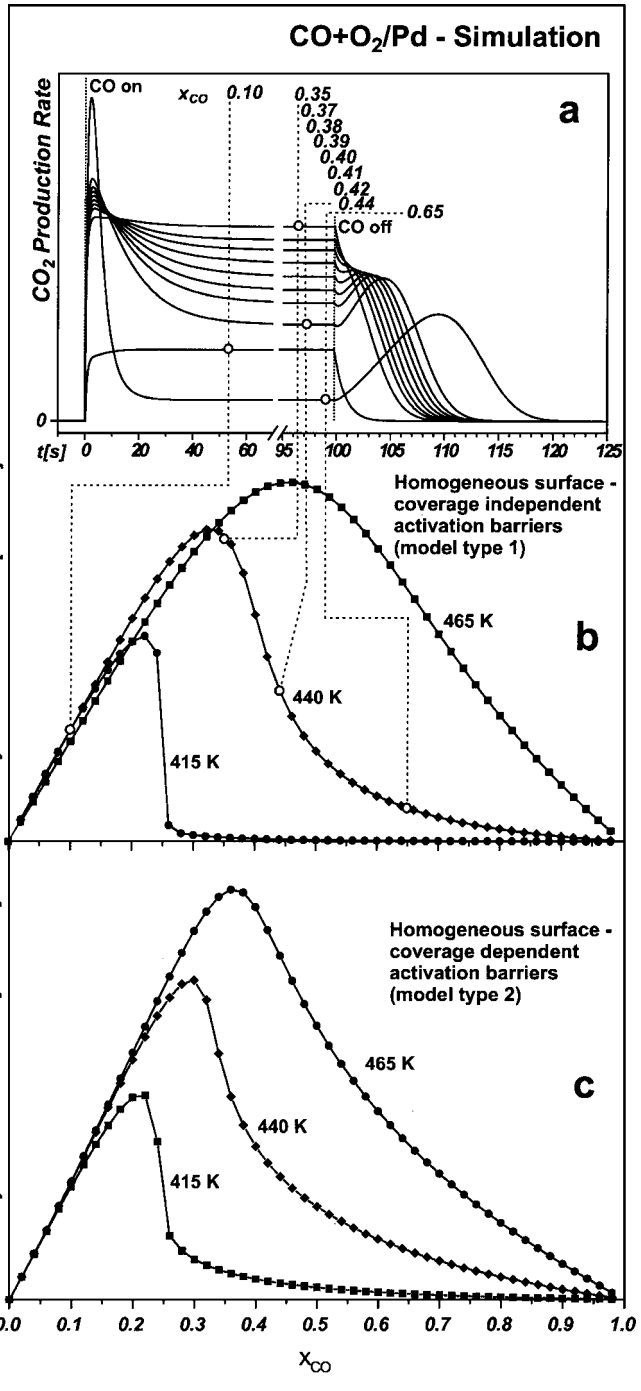

FIG. 4. (a) Simulated transient reaction rates for a homogeneous surface model with coverage-independent activation barriers (model type 1; for parameters see Table 2); (b) calculated steady-state rates for a homogeneous surface model with coverage-independent activation barriers (model type 1; for parameters see Table 2); (c) calculated steady-state rates for a homogeneous surface model with coverage-dependent activation barriers (model type 2; for parameters see Table 2).

A second deviation between the simple model and experimental results for the particles of type I is related to the temperature dependence of the steady-state reaction rates (see Figs. 1c and 4b). Whereas the decrease in the

reaction rate due to CO induced poisoning is well described for a surface temperature of 440 K, the effect is overestimated for lower and underestimated for higher temperatures. The differences can be related to the lateral interaction of the adsorbate molecules resulting in a pronounced coverage dependency of the CO adsorption energy (45) (model type 2). Within the most simple approximation we may take this effect into account by introducing a linearly coverage-dependent desorption energy (see also, e.g., (48))

$$E_{des} = E^0_{des}\left(1 - \alpha_{CO}\frac{\theta_{\mathrm{CO}}}{\theta^{\max}_{CO}}\right), \qquad [14]$$

with the zero coverage, desorption energy E^0_{des} and a relative coverage dependence and a coverage dependence coefficient α_{CO} (the choice of which sensitively depends on the coverage and temperature ranges to be considered). In the case of the Pd particles of type I we obtain a significantly improved description of the steady-state rates for all considered temperatures by choosing $\alpha_{CO} = 0.1$ (compare Figs. 4c and 1c). These values are, however, not intended to represent a fit to the experimental data, but to indicate the general trends. Also note that in case of strong lateral interactions and low sample temperatures the simple mean field model may no longer yield a good quantitative description due to the formation of nonhomogeneous adsorbate distributions (see, e.g.,(47)).

In spite of the more realistic steady-state behavior, it has to be pointed out that no homogeneous surface model provides a significantly improved description of the transient behavior. For this purpose a heterogeneous surface model is required as discussed in the following section.

3.2. Microkinetic Simulations: Heterogeneous Surface Models

We define a heterogeneous surface by assuming that the system consists of n different types of adsorption sites (e.g., different facets on one particle, defect-rich versus regular parts on one particle, or different particles with varying adsorption properties). Each of the types of adsorption sites covers a fraction α_i with $i = 1 \ldots n$ of the surface, which exposes a total density of N_{Pd} Pd surface atoms per unit area. We assume each of those sites to provide a complete reaction system, characterized by an individual set of kinetic parameters. Analogous to Eqs. [6]–[9] we obtain the reaction rate as

$$\frac{d\theta_{CO,i}}{dt} = \frac{F_{CO}}{N_{Pd}}S_{CO,i} - k_{des,i}\theta_{CO,i} - k_{LH,i}\theta_{CO,i}\theta_{O,i} \qquad [15]$$

$$\frac{d\theta_{O,i}}{dt} = 2\frac{F_{O_2}}{N_{Pd}}S_{O_2,i} - k_{LH,i}\theta_{CO,i}\theta_{O,i} \qquad [16]$$

$$r_{CO_2} = \frac{F_{CO_2}}{N_{Pd}} = \sum_i \alpha_i k_{LH,i}\theta_{CO,i}\theta_{O,i}; \quad i = 1 \ldots n. \qquad [17]$$

Here, we have defined the partial coverages of adsorption site i as

$$\theta_{CO,i} = \frac{N_{CO,i}}{\alpha_i N_{Pd}} \quad \theta_{O,i} = \frac{N_{O,i}}{\alpha_i N_{Pd}}. \qquad [18]$$

Furthermore, we define the site-specific activation energies and preexponentials for desorption $E_{des,i}$, $\nu_{des,i}$ and reaction $E_{LH,i}$, $\nu_{LH,i}$ and the site-specific, modified, Langmuir sticking coefficients $S^0_{CO,i}$ and $S^0_{O_2,i}$ analogous to Eqs. [10]–[13].

This model represents the limiting case in which there is no coupling by diffusion between the different adsorption sites (model type 3), and the total reaction rate is simply the sum over the isolated reactors of each type. This would, for example, be the case if metal particles with different properties would be separated by sufficiently large oxide areas, providing a large enough diffusion barrier or if diffusion of the adsorbate on the particle itself was slow with respect to the reaction.

As a second limiting case we may assume that surface diffusion of one of the adsorbates (i.e., the CO) is fast with respect to the adsorption and reaction step (model type 4). We will neglect surface diffusion of the second reactant (i.e., the atomically adsorbed oxygen, the diffusion of which is expected to be much slower than CO diffusion, see, e.g., (49). It should be noted, however, that no quantitative data are available on the surface diffusion coefficients of atomic oxygen on well-defined Pd surfaces. Presently, molecular beam experiments are performed in our group, which may provide indications on the time scale of oxygen diffusion over supported Pd particles).

Within the Langmuir adsorption model (i.e., neglecting lateral interactions and any influence of preadsorbed oxygen on the CO adsorption), we may write the chemical potential for the adsorbed CO on the sites of type i on a sufficiently large Pd particle as

$$\mu_{CO,i} = -kT \ln z_{CO,i} + kT \ln \frac{\theta_{CO,i}\theta^{\max^{-1}}_{CO,i}}{1 - \theta_{CO,i}\theta^{\max^{-1}}_{CO,i}} \qquad [19]$$

with the single particle partition function ($E_{ads,i}$ is the adsorption energy on site i):

$$z_{CO,i} = z^o_{CO,i}\varepsilon_i \quad \text{with} \quad \varepsilon_i = \exp\left(\frac{E_{ads,i}}{kT}\right). \qquad [20]$$

We assume that equilibrium is established via rapid surface diffusion. In this case we may write the equilibrium condition $\mu_{CO,i} = \mu_{CO,j}$ as

$$\frac{1 - \theta_{CO,i}\theta^{\max^{-1}}_{CO,i}}{\theta_{CO,i}\theta^{\max^{-1}}_{CO,i}} z^o_{CO,i}\varepsilon_i = \frac{1 - \theta_{CO,j}\theta^{\max^{-1}}_{CO,j}}{\theta_{CO,j}\theta^{\max^{-1}}_{CO,j}} z^o_{CO,j}\varepsilon_j \quad \forall\, i, j, \qquad [21]$$

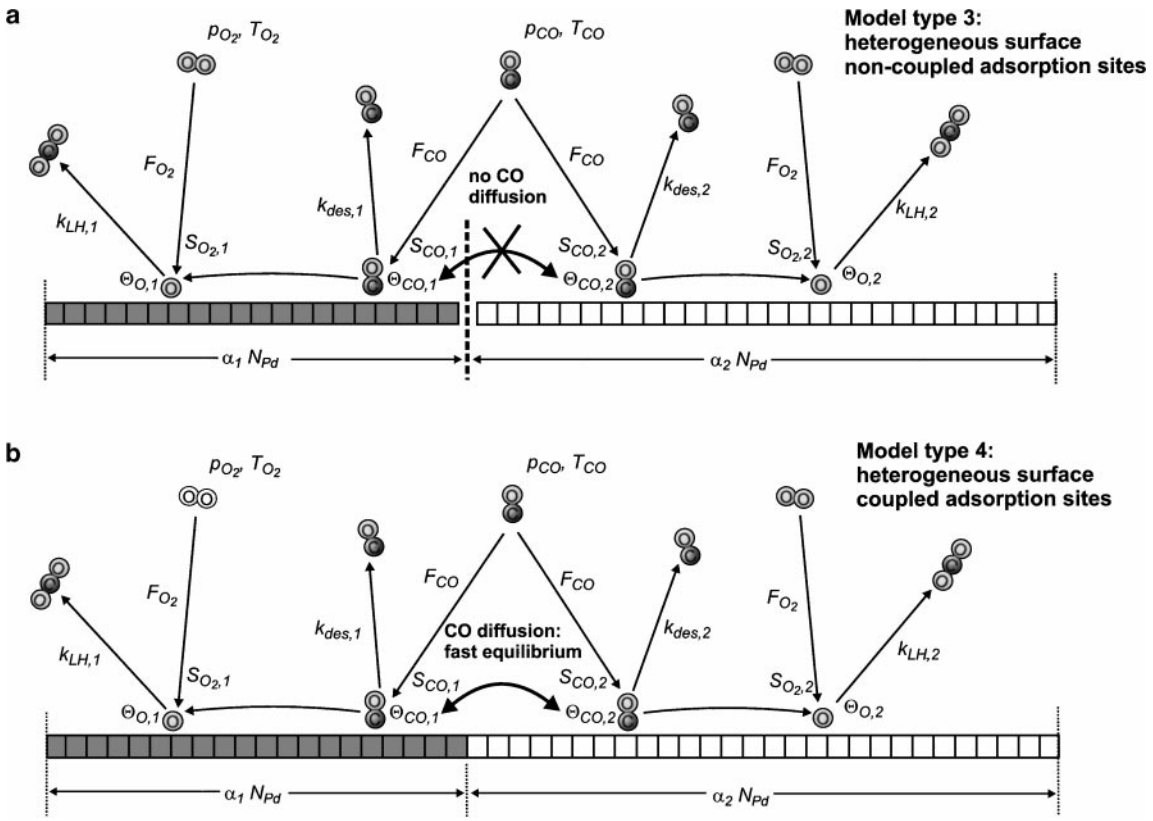

FIG. 5. Kinetic parameters in the heterogeneous surface models.

which has to be fulfilled under the condition of constant total coverage (i.e., adsorption, desorption and reaction are slow with respect to surface diffusion):

$$\frac{d}{dt}\frac{N_{CO}}{N_{Pd}} = \sum_i \alpha_i \frac{d}{dt}\theta_{CO,i} = 0. \qquad [22]$$

We may now simulate the kinetics by solving Eqs. [15]–[17] under the conditions of Eqs. [21]–[22].

At this point the model contains a large number of parameters, most of which are experimentally unknown. We may, however, consider a simplified case, which may at least guide us to a qualitative understanding of the observed particle size effects. As the most simple example we consider a surface containing only two types of adsorption sites ($i = 1, 2$). The situation is schematically depicted in Fig. 5. For simplicity we neglect differences in the internal, single particle, partition functions ($z^0_{CO,1} \approx z^o_{CO,2}$) and assume that the adsorption process is not activated ($E_{ads,i} = E_{des,i}$). From Eqs. [21] and [22] we obtain the following simple equilibrium and mass conservation conditions to be fulfilled when solving the kinetic equations:

$$\frac{\theta^{\max}_{CO,1} - \theta_{CO,1}}{\theta_{CO,1}} \cdot \frac{\theta_{CO,2}}{\theta^{\max}_{CO,2} - \theta_{CO,2}} = \exp\left(\frac{E_{des,2} - E_{des,1}}{kT}\right);$$

$$\alpha_1 \frac{d}{dt}\theta_{CO,1} + \alpha_2 \frac{d}{dt}\theta_{CO,2} = 0. \qquad [23]$$

As discussed in Section 2.1, it is known from previous adsorption studies that on the smaller particles there exists a large number of additional weakly CO binding sites, as compared to the single crystal surfaces (see Section 2.1, (6, 44)). We may therefore consider a situation in which a majority of regular adsorption sites (site type 1, see inset in Fig. 6a) coexists with a minority of more weakly CO adsorbing sites (site type 2). Based on a linear, free energy relationship argument, we may anticipate that the reduction in adsorption energy will also lead to a smaller reduction in the activation barrier for surface reaction. The parameters we have chosen for the simulation are listed in Table 2. In particular we use $\alpha_1 = 0.9$, $\alpha_2 = 0.1$ (10% defect adsorption sites) with the adsorption energies $E_{des,1} = 136$ kJmol^{-1}, $E_{des,2} = 110$ kJ mol^{-1}, and the activation energies $E_{LH,1} = 60$ kJ mol^{-1}, $E_{LH,2} = 45$ kJ mol^{-1} (for all other parameters, see Table 2). For the total Pd surface atom density we choose $N_{pd} = 0.54 \times 10^{15}$ cm^{-2} (which corresponds to the experimental value for the type I particles and is close to the value for the type II particles). Note that the value simply scales the effective flux of CO and O_2 per Pd surface atom at a given pressure. The choice corresponds to a situation, where a large fraction of the flux is trapped on the surface and diffuses to the particles. It should be pointed out that the choice of this parameter as well as the energetic parameters is arbitrary to a certain

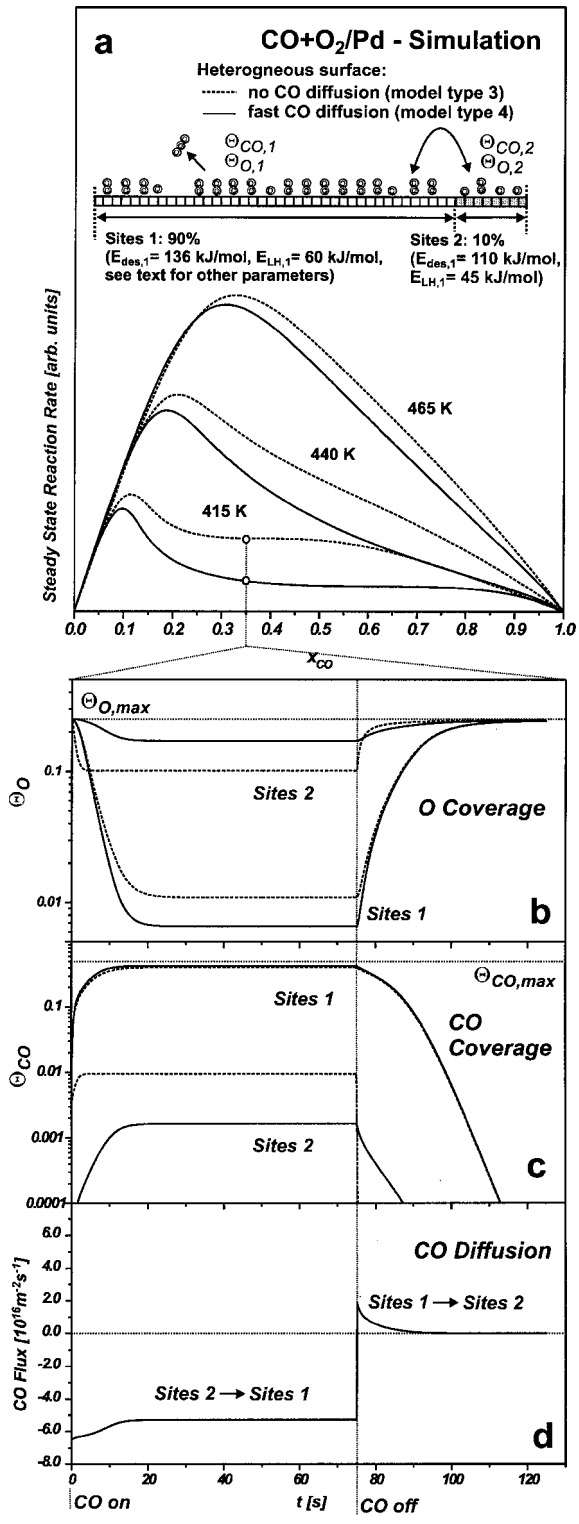

FIG. 6. (a) Simulated transient reaction rates ($p_{total} = 1.0 \times 10^{-6}$ mbar) for a heterogeneous surface without (dashed lines, model type 3) and with surface diffusion (solid lines, model type 4; for parameters see Table 2); (b) oxygen coverage of the adsorption sites of types 1 and 2 during a transient experiment at $x_{CO} = 0.35$ (dashed lines: without surface diffusion, model type 3; solid lines: with surface diffusion, model type 4, $T_S = 415$ K, $p_{total} = 1.0 \times 10^{-6}$ mbar; for other parameters see Table 2); same as in (b) for the CO coverage of the sites 1 and 2; (c) CO flux due to surface diffusion during the transient experiments.

extent. Their exact values are not intended to represent a fit of the experimental data. What is, however, essential in order to obtain the type of results shown in the following is that, in addition to the regular adsorption sites, we introduce a minority species of sites which bind CO more weakly. Under these conditions, the qualitative behavior does not critically depend on the exact choice of the parameters and, thus, the simulation may contribute to a qualitative understanding of the observed kinetics.

In Fig. 6a the calculated steady-state reaction rates for the two adsorption state models are shown for both possible models, disregarding CO diffusion (model type 3, dashed lines in Fig. 6) and taking CO diffusion into account (model type 4, solid lines in Fig. 6). The corresponding transient reaction rates are displayed in Fig. 7.

By comparison of the steady-state rates in Fig. 6 with those of the homogeneous surface in Fig. 4, it is immediately observed that within the heterogeneous surface model the CO poisoning effect at high CO fluxes is strongly reduced for both model cases (with and without CO diffusion). Moreover, in the case of weakly CO binding defect sites considered here, CO surface diffusion leads to a decrease in the steady-state reaction rates.

Both effects are easily understood, if we now examine the O and CO coverages (Figs. 6b and 6c) and the CO diffusion (Fig. 6d), which are established during a transient experiment of the type performed in this study. We choose slightly CO poisoning conditions ($x_{CO} = 0.35$). It is seen that CO-rich conditions are only established on sites of type 1, whereas the sites of type 2 remain in a O-rich steady state. Once we switch on CO diffusion, this effect is enhanced by CO migrating from the sites of type 2 to more strongly CO adsorbing sites of type 1 (see Fig. 6d). This effect leads to an enhanced poisoning of the sites of type 1 and CO depletion on sites 2, with both effects contributing to a decrease in the reaction rates. The direction of diffusion is only reversed immediately after the CO beam is switched off. The reversal is due to the reaction proceeding much faster on the sites of type 2 (due to the lower activation barrier and the high O coverage), which results in the sites of type 1 acting as a CO reservoir for reaction on sites of type 2.

Now it is interesting to consider the transient reaction rates for the heterogeneous surface models. The results for the diffusion coupled and nondiffusion coupled models are displayed in Fig. 7. It is noteworthy that for both model types we indeed observe the typical transition regime behavior—the dip in the reaction rate upon switching off the CO beam followed by a CO_2 production peak—over quite a broad range of flux conditions. Also, the steady-state reaction rate is higher with respect to the transient peak as compared to the homogeneous surface model (compare to Fig. 4). A closer inspection of the transients reveals that the dip appears more pronounced in the case of the nondiffusion coupled system (model type 3) in comparison with the coupled system (model type 4). This is due to the surface

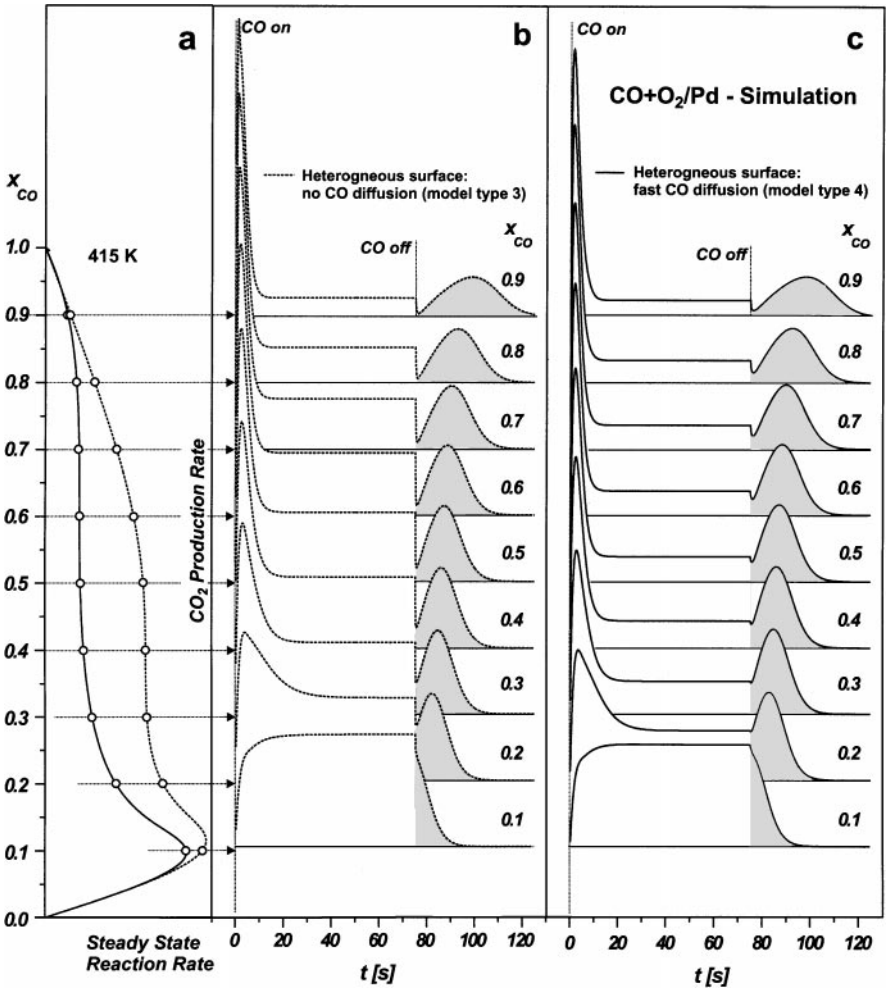

FIG. 7. (a) Simulated steady-state reaction rates ($p_{total} = 1.0 \times 10^{-6}$ mbar, $T_S = 415$ K) for a heterogeneous surface without (dashed lines, model type 3) and with surface diffusion (solid lines, model type 4; for other parameters see Table 2); (b) corresponding transient reaction rates for a model without surface diffusion (model type 3); corresponding transient reaction rates for a model with surface diffusion (model type 4).

diffusion of CO from the sites of type 1 to the sites of type 2 after the CO beam is switched off, which was already discussed above. The coupling to the CO reservoir on the sites of type 1 maintains a high reaction rate on the sites of type 2 after termination of the CO flux, whereas for the noncoupled system (model type 3) fast consumption of the CO on sites of type 2 results in a very rapid drop and thus a more pronounced dip in the rate.

At this point we may conclude that all differences observed in the transient and steady-state kinetics for the small particles (type 2) in comparison to the larger and ordered particles of type 1 are qualitatively reflected by the heterogeneous surface model. Specifically, these effects are (a) the reduced poisoning under CO-rich conditions, (b) the appearance of a pronounced dip in the transient reaction rate over a very large range of flux conditions, and (c) increased steady-state reaction rates in comparison with the transient CO_2 peaks.

In general, these differences are all related to the effect that due to its modified CO adsorption properties, a fraction of the heterogeneous particle surface (the sites of type 2) remains in an oxygen-rich state, even under conditions under which the single crystal surface would already be CO poisoned. Thus, these sites open an additional channel for oxygen adsorption and help to maintain a high reaction rate even under CO-rich conditions.

With respect to the transient dip in the reaction rate, it has to be pointed out that the sudden decrease in the reaction rate should indeed not be related to a sudden change in the CO coverage. Instead, it becomes clear from Fig. 6 that the effect is mainly connected to a decrease in the CO coverage on the weakly CO adsorbing sites of type 2, which, however, always remain in a O-rich and CO-poor state and, additionally, represent the minority species. Thus, their contribution to the total CO coverage is negligible. This immediately explains the experimental observation that the sudden change

in the reaction rate was not found to be correlated to a sudden change in the IR absorption spectra (see Section 2.2 and (35)).

Finally we may remark that both heterogeneous surface models (including and not including surface diffusion) qualitatively give rise to similar kinetic effects, which match the experimental observations on the small particles. At this point, a preferential assignment to either of these models cannot be provided. Such an assignment would require an exact quantitative treatment based on a number of kinetic parameters, which are not available at this point. Moreover, numerous additional contributions, e.g., due to adsorption on the support, specific diffusion barriers, or the local distribution of sites, may have to be included in a quantitative treatment. With the help of a detailed structural characterization in combination with suitable transient and steady-state kinetic probes, we may, however, approach a situation where such microkinetic models for highly complex surfaces could become available and may provide a very detailed insight into the kinetics on these systems.

4. CONCLUSIONS

In conclusion we have employed multimolecular beam techniques to study the transient and steady-state kinetics of the CO oxidation on a Pd/Al_2O_3 model catalyst. The catalysts are prepared under UHV conditions by oxidizing a NiAl(110) single crystal to form a well-ordered Al_2O_3 film and subsequent deposition of Pd under well-controlled conditions. Previously, these systems have been characterized in detail with respect to their geometric and electronic structure and their morphology.

(1) We have compared the CO oxidation kinetics over two types of model catalysts, which are characterized by Pd particle sizes of 5.5 nm (type I) and 1.8 nm (type II), respectively. Whereas the smaller particles (type II) expose a high density of defect sites, the larger particles (type I) represent well-ordered crystallites, which grow in (111) orientation and are largely terminated by ordered (111) facets and a small fraction of (100) facets.

(2) The partial pressures of the reactants have been applied by crossing two molecular beams on the sample surface. We have systematically probed the CO_2 production rate under steady-state and transient conditions over a wide range of CO/O_2 ratios and at different sample temperatures. Previously, these experiments were correlated with time-resolved in situ, IR, reflection absorption spectroscopy measurements.

(3) Clear differences are observed for the two types of Pd particles, both under transient and steady-state conditions. With respect to the transient behavior the differences are mainly related to the kinetics upon termination the CO flux at constant O_2 flux. For the small particles (type II) a characteristic dip in the reaction rate is observed over a broad range of flux conditions, whereas such a behavior is less pronounced and limited to a very narrow range of conditions for the large particles (type I). With respect to the steady-state rates, we find that for the small particles (type II) the CO induced poisoning of the surface is strongly suppressed.

(4) We have simulated both the transient experiments and the steady-state reaction rate as a function of temperature and reactant fluxes on the basis of simple mean field models. In general, the reaction rates on the large particles are reasonably well described by a homogeneous surface model. This holds with the exception of the transient behavior in the transition region between the oxygen-rich and CO-rich reaction conditions. We suggest that the deviations are related to the remaining heterogeneity of the supported model catalyst, i.e., the variations in island sizes, distances, and morphologies.

(5) In order to qualitatively understand the differences in the kinetics for the two types of Pd particles, we consider a heterogeneous surface model, which takes into account the simultaneous presence of different types of adsorption sites. Depending on the type of heterogeneity, we include surface diffusion between these sites. Specifically, we assume the presence of additional weakly CO adsorbing sites, which is in agreement with previous adsorption studies. The differences observed for the small particles (type II) with respect to both the transient and steady-state reaction rates can be qualitatively understood by this simple model. Moreover, the transient development of the CO coverage is in agreement with previous time-resolved, in situ IRAS measurements.

ACKNOWLEDGMENTS

This project has been funded by the Max-Planck Society and the Deutsche Forschungsgemeinschaft. We thank Dr. M. Frank and Dr. M. Bäumer for STM data used in this work. Moreover, we would like to acknowledge many useful discussions with Prof. C. R. Henry and Dr. L. Piccolo in the initial stages of this project.

REFERENCES

1. Bond, B. C., *Surf. Sci.* **156**, 966 (1985).
2. Zhdanov, V. P., and Kasemo, B., *Surf. Sci. Rep.* **39**, 25 (2000).
3. Zhdanov, V. P., and Kasemo, B., *Surf. Sci.* **405**, 27 (1998).
4. Zhdanov, V. P., and Kasemo, B., *J. Catal.* **170**, 377 (1997).
5. Henry, C. R., *Surf. Sci. Rep.* **31**, 231 (1998).
6. Bäumer, M., and Freund, H.-J., *Prog. Surf. Sci.* **61**, 127 (1999).
7. Rainer, D. R., and Goodman, D. W., *J. Mol. Catal. A* **131**, 259 (1998).
8. Freund, H.-J., *Angew. Chem. Int. Ed. Engl.* **36**, 452 (1997).
9. Bäumer, M., Libuda, J., and Freund, H.-J., *in* "Chemisorption and Reactivity on Supported Clusters and Thin Films" (M. Lambert and G. Pacchioni, Eds.), p. 61. Kluwer Academic, Dordrecht/Norwell, MA, 1997.
10. Jaeger, R. M., Kuhlenbeck, H., Freund, H.-J., Wuttig, M., Hoffmann, W., Franchy, R., and Ibach, H., *Surf. Sci.* **259**, 235 (1991).
11. Libuda, J., Winkelmann, F., Bäumer, M., Freund, H.-J., Bertrams, T., Neddermeyer, H., and Müller, K., *Surf. Sci.* **318**, 61 (1994).

12. Frank, M., and Bäumer, M., *Phys. Chem. Chem. Phys.* **2**, 4265 (2000).
13. Asscher, M., and Somorjai, G. A., *in* "Atomic and Molecular Beam Methods" (G. Scoles, Ed.), Vol. 2, p. 489. Oxford Univ. Press, London, 1988.
14. D'Evelyn, M. P., and Madix, R. J., *Surf. Sci. Rep.* **3**, 413 (1984).
15. Rettner, C. T., Auerbach, D. J., Tully, J. C., and Kleyn, A. W., *J. Phys. Chem.* **100**, 13,021 (1996).
16. Piccolo, L., Becker, C., and Henry, C. R., *Appl. Surf. Sci.* **164**, 156 (2000).
17. Henry, C. R., *Appl. Surf. Sci.* **164**, 252 (2000).
18. Becker, C., and Henry, C. R., *Catal. Lett.* **43**, 55 (1997).
19. Becker, C., and Henry, C. R., *Surf. Sci.* **352**, 457 (1996).
20. Henry, C. R., Chapon, C., Goyhenex, C., and Monot, R., *Surf. Sci.* **272**, 283 (1992).
21. Duriez, C., Henry, C. R., and Chapon, C., *Surf. Sci.* **253**, 191 (1991).
22. Henry, C. R., Chapon, C., and Duriez, C., *Z. Phys. D* **19**, 347 (1991).
23. Henry, C. R., Chapon, C., and Duriez, C., *J. Chem. Phys.* **95**, 804 (1991).
24. Matolin, V., and Stara, I., *Surf. Sci.* **398**, 117 (1998).
25. Jungwirthova, I., Stara, I., and Matolin, V., *Surf. Sci.* **377**, 644 (1997).
26. Stara, I., and Matolin, V., *Surf. Sci.* **313**, 99 (1994).
27. Stará, I., Nehasil, V., and Matolín,V., *Surf. Sci.* **331–333**, 173 (1995).
28. Nehasil, V., Hrncir, T., Zafeiratos, S., Ladas, S., and Matolin, V., *Surf. Sci.* **454**, 289 (2000).
29. Nehasil, V., Stara, I., and Matolin, V., *Surf. Sci.* **377**, 813 (1997).
30. Nehasil, V., Stara, I., and Matolin, V., *Surf. Sci.* **352**, 305 (1996).
31. Piccolo, L., and Henry, C. R., *Appl. Surf. Sci.* **162–163**, 670 (2000).
32. Piccolo, L., and Henry, C. R., *Surf. Sci.* **452**, 198 (2000).
33. Meusel, I., Hoffmann, J., Hartmann, J., Heemeier, M., Bäumer, M., Libuda, J., and Freund, H. J., *Catal. Lett.* **71**, 5 (2001).
34. Dellwig, T., Hartmann, J., Libuda, J., Meusel, I., Rupprechter, G., Unterhalt, H., and Freund, H.-J., *J. Mol. Catal. A* **162**, 51 (2000).
35. Libuda, J., Meusel, I., Hoffmann, J., Hartmann, J., Piccolo, L., Henry, C. R., and Freund, H.-J., *J. Chem. Phys.* **114**, 4669 (2001).
36. Meusel, I., Hoffmann, J., Hartmann, J., Libuda, J., and Freund, H.-J., *J. Phys. Chem. B* **105**, 3567 (2001).
37. Libuda, J., Meusel, I., Hoffmann, J., Hartmann, J., and Freund, H.-J., *J. Vac. Sci. Technol. A* **19**, 1516 (2001).
38. Bäumer, M., Libuda, J., Sandell, A., Freund, H.-J., Graw, G., Bertrams, T., and Neddermeyer, H., *Ber. Bunsenges. Phys. Chem.* **99**, 1381 (1995).
39. Hansen, K. H., Worren, T., Stempel, S., Laegsgaard, E., Bäumer, M., Freund, H.-J., Besenbacher, F., and Stensgaard, I., *Phys. Rev. Lett.* **83**, 4120 (1999).
40. Shaikhutdinov, S., Heemeier, M., Hoffmann, J., Meusel, I., Richter, B., Bäumer, M., Kuhlenbeck, H., Libuda, J., Freund, H.-J., Oldman, R., Jackson, S. D., Konvicka, C., Schmid, M., and Varga, P., *Surf. Sci.*, submitted for publication.
41. Hammer, B., *J. Catal.* **199**, 171 (2001).
42. Libuda, J., Meusel, I., Hartmann, J., and Freund, H.-J., *Rev. Sci. Instrum.* **71**, 4395 (2000).
43. Engel, T., and Ertl, G., *in* "The Chemical Physics of Solid Surfaces and Heterogeneous Catalysis" (D. A. King and D. P. Woodruff, Eds.), Vol. 4, p. 73. Elsevier, Amsterdam/New York, 1982.
44. Bäumer, M., Frank, M., Libuda, J., Stempel. S., and Freund, H.-J., *Surf. Sci.* **391**, 204 (1997).
45. Guo, X., Hoffman, A., and Yates, J. T., Jr., *J. Chem. Phys.* **90**, 5787 (1989).
46. Engel, T., and Ertl, G., *J. Chem. Phys.* **69**, 1267 (1978).
47. Wintterlin, J., Völkening, S., Janssens, T. V. W., Zambelli, T., and Ertl, G., *Science* **278**, 1931 (1997).
48. Eriksson, M., and Ekedahl, L.-G., *Surf. Sci.* **412/413**, 430 (1998).
49. Seebauer, E. G., and Allen, C. E., *Prog. Surf. Sci.* **49**, 265 (1995).
50. Engel, T., *J. Chem. Phys.* **69**, 373 (1978).
51. Conrad, H., Ertl, G., and Küppers, J., *Surf. Sci.* **76**, 323 (1978).